J Polym Res (2014) 21:349
DOI 10.1007/s10965-013-0349-4

ORIGINAL PAPER

Preparation, characterization, and antibacterial properties of pH-responsive P(MMA-co-MAA)/silver nanocomposite hydrogels

Qing-Bo Wei · Feng Fu · Yu-Qi Zhang · Long Tang

Received: 8 August 2013 / Accepted: 26 December 2013 / Published online: 9 January 2014

Abstract A pH-responsive copolymer hydrogel was synthesized based on methyl methacrylate (MMA) and methacrylic acid (MAA) as monomers, and was adopted as a nanoreactor for assembling Ag nanoparticles. Fourier transform infrared spectroscope (FTIR), scanning electron microscopy (SEM), transmission electron microscope (TEM), UV-visible spectroscopy (UV-Vis) and thermogravimetric analysis (TGA) were used to fully characterize the formation of silver nanoparticles in P(MMA-co-MAA) hydrogels. The experimental results showed that the P(MMA-co-MAA) hydrogels assume a three-networks architecture in morphologies, and that nearly spherical Ag nanoparticles are formed in these hydrogel networks; the size of these Ag nanoparticles varies with the system composition. The swelling kinetics investigations demonstrated that the equilibrium swelling ratio (ESR) of the P(MMA-co-MAA)/Ag hydrogels depended on the content of the MAA and pH of the buffer solutions, and the ESR values were reduced with increasing MAA contents. The antibacterial properties against both *S. aureus* and *B. subtilis* bacteria demonstrated that the P(MMA-co-MAA)/silver nanocomposite hydrogels had higher antimicrobial efficacy than the pure P(MMA-co-MAA) counterparts. Therefore, the nanocomposite hydrogels turned out to be a potentially smart material in the range of applications of antibacterial activity.

Keywords Hydrogels · Ag nanoparticles · Nanocomposites · Swelling · Antibacterial activities

Q.-B. Wei (✉) · F. Fu (✉) · Y.-Q. Zhang · L. Tang
Key Laboratory of Chemical Reaction Engineering of Shaanxi Province, College of Chemistry & Chemical Engineering, Yan'an University, Yan'an 716000, People's Republic of China
e-mail: qbwei2011@126.com
e-mail: yadxgncl@126.com

Introduction

As is known to all, metal nanoparticles possess a wide range of unique physical properties, e.g., electrical, optical, magnetic, etc., due to their intermediate structures between atomic state and the bulk [1–3]. Silver nanoparticles (AgNPs) are intensively studied for their potential use in catalysis, biosensors, biomedicine, and environmental filtration [4–7]. The bactericidal and inhibitory effects of silver nanoparticles against a wide range of microorganisms are well documented. Since these performances have a considerable association with the structure, surface modality, size, and size distribution, a strict control is needed. A versatile system must show antibacterial activity toward germs on contact without release of toxic biocides; the antimicrobial properties of AgNPs are considered non-toxic and environmentally friendly in biomedical applications. Polymer matrices can prevent oxidation and coalescence of the particles and provide them with long-time stability. Therefore, the AgNPs/polymer composite, functioning as a bactericide, has been applied in complicated cases of infected burns, purulent wounds, and as a wound-healing matrix [8, 9]. Up to now, several methods have been established for the preparation of various silver-polymer nanocomposites [10–14] including physical techniques such as thermal evaporation and laser sputtering, and chemical techniques such as in-situ chemical reduction ($NaBH_4$), refluxing and heating methods, bio-reduction, X-ray irradiation, and layer-by-layer assembly, etc. However, due to their poor binding characteristics with surfaces of antibacterial materials, their utility has been restricted. Therefore, polymer-stabilized nanoparticles, especially nanoparticles embedded in hydrogel networks, are outstanding approaches for antibacterial applications [8, 15–17]. A silver-impregnated polymer matrix provides antimicrobial efficacy with a sustained release of silver. The silver/polymer fabric minimizes the transmission of

infective agents and enhances patient comfort, and offers a facile application for health care.

Polymer hydrogels may be defined as crosslinked three-dimensional polymer networks swollen with water or biological fluids. They can offer large free space between the crosslinked networks in the swollen stage as a nanoreactor template for the nucleation and growth of Ag nanoparticles. Many reseachers have reported their work using polymer hydrogels as nanoreactors for uniform distribution of AgNPs [18–20]. These hydrogels include carboxymethyl cellulose-based hydrogels, chitosan–polyvinyl alcohol hydrogel, and poly(acrylic acid), etc. Since they have structural similarity to the macromolecular-based components in the body, they are considered biocompatible [21]. Poly(methacrylic acid) (PMMA) hydrogel as a biocompatible polymer is typically used in the fabrication of contact lenses, etc. [22]. Polymethacrylic acid (PMAA) hydrogel is a typical pH-responsive hydrogel, and has received considerable recognition in biomedical applications due to good biocompatibility [23–25]. Considering that the biological activity of AgNPs, especially the antibacterial property, is dependent on the size of particles and the swelling ratio [26], it is important to design and construct new copolymer hydrogels with adjustable network dimension and swelling ratios. To this end, constructing poly(methyl methacrylate-co-methacrylic acid) (P(MMA-co-MAA)) copolymer networks by copolymerization of MMA and MAA monomers with various component ratios may be a suitable choice. Thus, not only the network size and swelling behavior may be mediated, but the interactions between functional groups in PMMA and PMAA chains and Ag^+ cations are controllable as well, which is helpful for assembling of Ag nanoparticles.

Based on the above description, the objective of this contribution is to synthesize pH-sensitive P(MMA-co-MAA) hydrogels with tunable MMA/MAA component ratios via free radical copolymerization. In the meanwhile, Ag nanoparticles were assembled in the copolymer hydrogels as nanoreactor templates, where functional groups in PMMA and PMAA chains can couple with Ag^+ cations by a complexation or electrostatic interaction and make the Ag nanoparticles efficiently stabilize. Compared with any other work reported [18–20], the innovativeness, or novelty, of this article is that pH-responsive P(MMA-co-MAA)/Ag nanocomposite hydrogels with tunable size of AgNPs are achieved. This hydrogel bears improved antibacterial efficacy by manipulating and controlling swelling ratios or/and feed ratios of the hydrogels and the size of Ag nanoparticles. So far, there is no literature reporting synthesis of silver nanoparticles employing P(MMA-*co*-MAA) hydrogels. Therefore, we herein report onnanocomposite hydrogels as promising antibacterial materials.

Experimental section

Materials and reagents

The analytical grade (AR) methyl methacrylate (MMA) was purchased by the Tianjin Kermol Chemical Regent Developing Center (Tianjin, People's Republic of China) and distilled two times prior to use in order to remove inhibitors and trace water. The methacrylic acid (MAA), analytical grade (AR), was supplied by the Tianjin Jinyu Fine Chemicals Ltd., Corp. (Tianjin, People's Republic of China). The cross-linker, N, N-methylenebisacrylamide (NNMBA, AR), was purchased by the Tianjin Kermol Chemical Regent Developing Center. Potassium persulfate (KPS) was recrystallized before use as an initiator. $AgNO_3$, AR, was supplied by the Shanghai Institute of Fine Chemicals and Industrial Materials (Shanghai, People's Republic of China). Sodium hypophosphite ($NaH_2PO_2{\cdot}H_2O$), used as a comparative reducer, was purchased by the Beijing Chemical Factory (Beijing, People's Republic of China).

Preparation of P(MMA-co-MAA) co-polymer network hydrogels

P(MMA-co-MAA) hydrogels were synthesized by a free radical cross-linking co-polymerization approach at a mass ratio of MMA to MAA of 30:70, 40:60, 50:50, 60:40 and 70:30, respectively. Stoichiometric MMA and MAA monomers were added in 20 ml deionized water. After the mixture solution was stirred at 60 °C for about 30 min, 0.02 g KPS and 0.02 g 1 wt.% NNMBA were added to the reaction mixture with rapid stirring. The reaction proceeded at 60 °C for about 2 h. The products were immersed with deionized water for 7 days to remove residues of the unreacted monomers, initiators, and cross-linking agents. The resultant hydrogels were dried in a vacuum at 35 °C until constant weight.

Assembly of Ag nanoparticles in P(MMA-co-MAA)/Ag hydrogel networks

The assembly of Ag nanoparticles in semi-IPN P(MMA-co-MAA) hydrogel networks has been performed in the following steps. Dry hydrogels were equilibrated with water for 3 days. Then the swollen hydrogels were transferred into a beaker containing 50 ml of 0.5 M $AgNO_3$ aqueous solution to diffuse for 1 day. These hydrogels loaded with sliver salts were subsequently transferred into a 50 ml 0.5 M $NaH_2PO_2{\cdot}H_2O$ aqueous solution was employed to reduce the sliver ions into silver nanoparticles at room temperature for 24 h. The sliver nanoparticles assembled in the hydrogel networks are often termed as P(MMA-co-MAA)/Ag nanocomposite hydrogels. The products were dried in a vacuum at 35 °C until constant weight. A structural model suggested

expatiating upon the fabrication of P(MMA-co-MAA)/Ag nanoparticles, and the applications for antibacterial activity were displayed in Scheme 1.

Measurements and characterization

To understand the swelling of P(MMA-co-MAA)/Ag nanocomposite hydrogels with varying compositions, the dried hydrogels (W_0) were immersed in an excess amount of deionized water at 25 °C until swelling equilibrium was attained. The wet weight of the sample (W_t) was determined after removing the surface water by blotting with filter paper, and the equilibrium water content was designated as W_∞. The swelling ratio (S_R) and equilibrium swelling ratios (ESR) of the samples were calculated from the following equations:

$$S_R = (W_t - W_0)/W_0 \quad (1)$$

$$ESR = (W_\infty - W_0)/W_0 \quad (2)$$

Antimicrobial tests

Bacteria (Staphylococcus aureus and Bacillus subtilis) strains were provided by the College of Life Sciences at Northwest University (People's Republic of China). The antimicrobial activities of P(MAA-co-MMA) and P(MAA-co-MMA)/Ag were examined by the bacteriostatic ring test method. The antibacterial activity was measured as the diameter of the inhibitory zones in the soft agar layer stained after 48 h incubation at 37 °C. An inhibitory zone with a diameter less than 16 mm corresponds to lack of activity (16 mm is the diameter of the spot). Control experiments with solvents show that the solvents have no activity.

Results and discussion

FT-IR

Figure 1 illustrates FTIR spectra of different P(MMA-co-MAA) pure hydrogels and P(MMA-co-MAA)/Ag nanocomposite hydrogels. As shown in Fig. 1. The poly(MMA-co-MAA) hydrogels and P(MMA-co-MAA)/Ag exhibited a relatively strong vibration band at 3600-3100 cm^{-1} due to the –OH group on the MAA moiety and the $–NH_2$ on the NNMBA cross-linker. The vibration absorption peaks at approximately 2910-2925 cm^{-1} are attributed to the stretch vibration mode of $–CH_3$ and $–CH_2–$ groups. The different samples of peaks at 1690-1731 cm^{-1} are ascribed to C=O stretching vibration, indicating that –C=O– groups are present in MMA and MAA. From Fig. 1(a, b, and c), as the content of MAA increases, –OH stretching vibration peak becomes sharp from the wide and blue shift. It is found that the characteristic absorptions of pure hydrogel and P(MMA-co-MAA)/Ag composite are quite similar except for the –OH stretching absorption bands; the

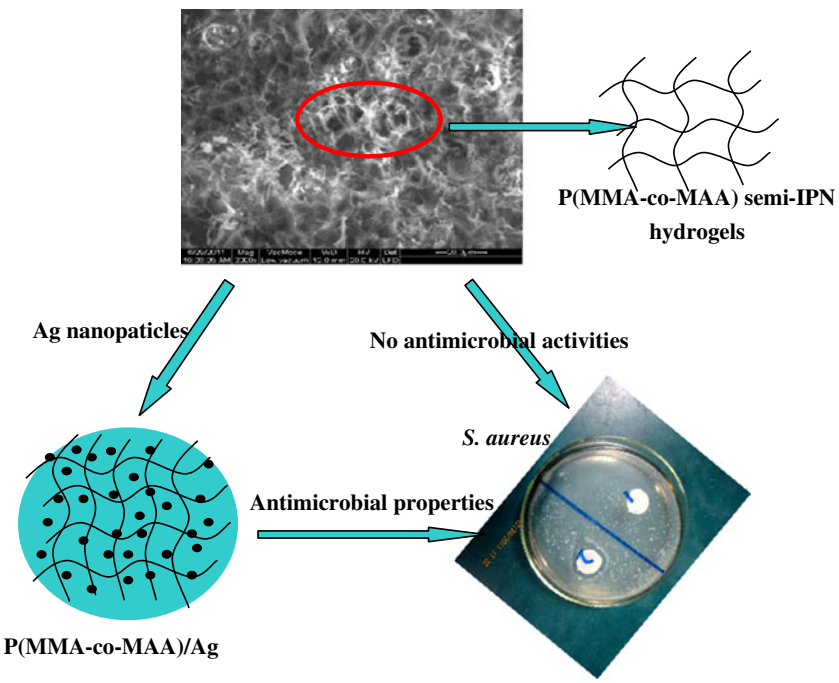

Scheme 1 A structural model suggested expatiating upon the fabrication of P(MMA-co-MAA)/Ag hydrogels, and the antibacterial studies (Antibaterial activities of (1) pure and (2) nanocomposite hydrogels against S. aureus).

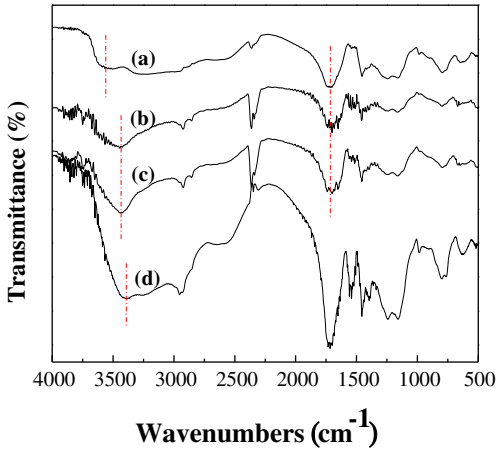

Fig. 1 FTIR spectra of P(MMA-co-MAA) various pure hydrogels [*a* (40/60), *b* (50/50), *c* (70/30)] and P(MMA-co-MAA)/Ag nanocomposite hydrogel [mass ratios of MMA to MAA: *d* (50/50)]

blue shift of the –OH stretching peak implies that the interaction also exists between the Ag nanoparticles and –COO– groups. In Fig. 1(d) the P(MMA-co-MAA)/Ag sample gave rise to a variational characteristic peak position and decreased transmittance owing to a chemical environment change resulting from the embedding of Ag nanoparticles by forming a complex between Ag/Ag^+ and the carboxyl groups [27]. Therefore, these findings preliminarily indicate that the P(MMA-co-MAA) has been synthesized, and Ag nanoparticles have been fabricated in the P(MMA-co-MAA) hydrogels, resulting in the P(MMA-co-MAA)/Ag nanocomposite.

SEM observations

Figure 2 shows SEM micrographs of the surfaces of both the pure P(MMA-co-MAA) hydrogels and P(MMA-co-MAA)/Ag gels, which were in the fully swollen state. It can be seen that P(MMA-co-MAA) hydrogels have porous structures with pores of micrometer size. The SEM micrographs clearly illustrate the morphological dependence on the different ratio of MMA to MAA in the hydrogels. Although the network topologies of the three control samples in Fig. 2(a–c) seem to be almost the same, the construction units of the networks appear to be different. It can be seen from Fig. 2 that pure P(MMA-co-MAA) hydrogels exhibited a characteristic three-dimensional honeycomb-like pattern. However, with increases of the MAA contents in the hydrogel composition, Fig. 2(a) and (b) have more uniform and dense pores in comparison with (c). It was clear that the pores of the gel in Fig. 2(c) were deeper and larger than those of the gels in (a) and (b). These hydrogel networks may be considered as templates to construct or assemble metal Ag nanoparticles. In the P(MMA-co-MAA)/Ag nanocomposite hydrogel morphologies exhibited by Fig. 2(d–f), it seems that Ag particles of nearly spherical shapes are assembled or attached on the surface of the hydrogels, which may be inferred from the SEM differences between the control samples and the nanocomposite hydrogels. Of course, a small amount of Ag nanoparticles can be observed in the hydrogel networks and on the surface. The application of using a free radical co-polymerization method to prepare pure P(MMA-co-MAA) hydrogels gave the hydrogels a more porous structure. This developed, porous structure of the hydrogels would act as a nanoreactor for preparation of Ag nanoparticles and make water diffusion into or out of its network easier during the deswelling–reswelling process. An energy dispersive X-ray detector attached to the SEM was used to measure Ag nanoparticles, and the content of Ag nanoparticles decreased. All these factors modulate and control the size of the nanoparticles and supply better stabilization of Ag nanoparticles. That is, the Ag nanoparticles are bound to grow or aggregate in the compartment of the copolymer templates in line with the orientation of preferential growth of a crystal plane.

TEM observations

From the TEM images in Fig. 3, it is readily observed that the morphologies of all the prepared Ag nanoparticles are either of a spherical or rectangular shape. The Ag nanoparticles generated by a direct reduction of $AgNO_3$ using sodium hypophosphite as a reducing agent are exhibited in Fig. 3(a). We notice that the Ag nanoparticles assembled in P(MMA-co-MAA) hydrogel networks with $NaH_2PO_2{\cdot}H_2O$ used as reducer. From TEM images in Fig. 3(b) and (c), these Ag particles assume spherical-like shape in appearance at nanoscale levels, and the size varies with the system composition (i.e., mass ratios of MMA to MAA). The probability is that the hydrogel networks not only make for better surface protection and a strong localization of Ag nanoparticles, but also can control the growth of Ag nanoparticles within the gel networks. It is known that Ag^+ can combine with oxygen and nitrogen atoms existing in the hydrogel networks via a weak coordination bond, forming $O\text{-}Ag^+$ and/or $N\text{-}Ag^+$ σ coordination bonds, and thus astricting Ag^+ particles, as narrated above. Therefore the Ag^+ ions may uniformly be fixed and distributed in the hydrogel networks [28]. The hydrogel networks have substantial impact on the formation of Ag nanoparticles, which not only make for surface protection and strong localization of Ag nanoparticles, but also can be adopted to control the growth of Ag nanoparticles within the gel networks. The electrostatic interaction (i.e., ion-dipole) between the electron-rich (ether) oxygen atoms of polar hydroxyl groups and/or carbonyl groups and electropositive transition metal cations is another factor affecting the Ag grain morphologies [29]. All of these help in modulating and controlling the size of the nanoparticles and supplying better stabilization of Ag nanoparticles. The optical properties of P(MMA-co-MAA)/Ag

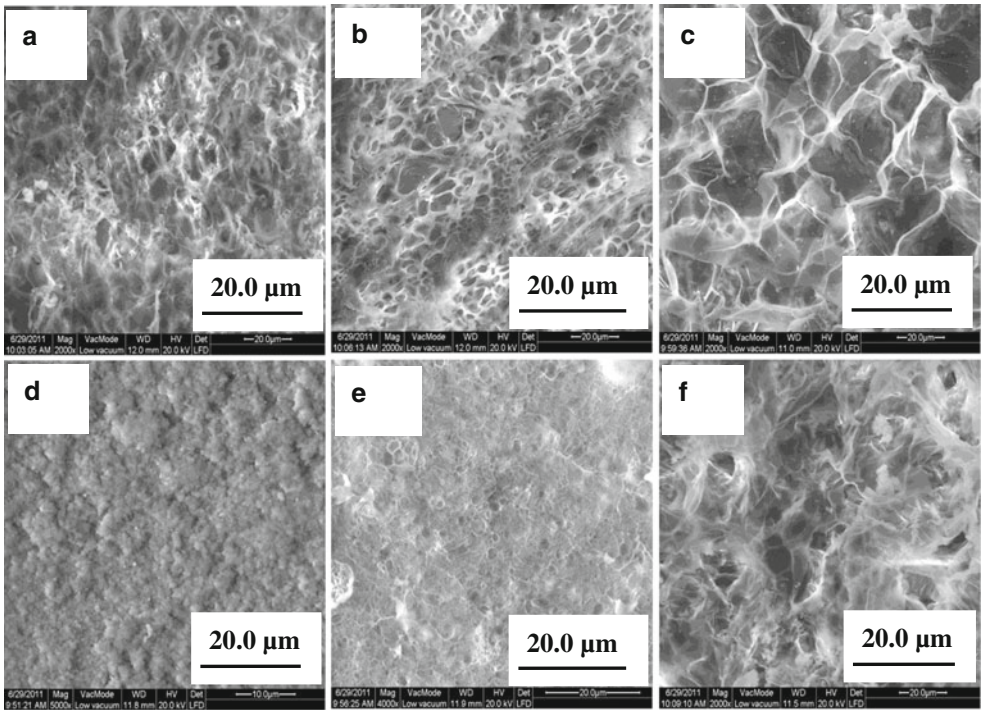

Fig. 2 SEM photographs of various hydrogels: **a**–**c** and **d**–**f**, Pure hydrogels (**a**–**c**) with different mass ratios of MMA to MAA: **a** 30:70, **b** 50:50, **c** 70:30; Control samples; (**d**–**f**). P(MMA-co-MAA)/Ag composite hydrogels prepared by in situ reducing Ag^{+} ions with $NaH_2PO_2{\cdot}H_2O$

nanocomposites and the size of Ag nanoparticles will be further evaluated by UV–Vis absorption spectra.

Optical properties

The optical properties of P(MMA-co-MAA)/Ag nanocomposites and the size distribution of Ag nanoparticles are further evaluated by UV-Vis absorption spectra. For UV-Vis studies, well-dispersed P(MMA-co-MAA)/Ag solutions were filled in a 1 cm path-length quartz cuvette and the spectra were recorded on a UV-Vis spectrometer using deionized water for background correction. Figure 4 shows the UV-Vis absorption spectra of P(MMA-co-MAA)/Ag nanocomposite samples obtained at different ratios of MMA to MAA. It can be seen that the recorded spectra show the presence of an absorption peak at about 420 nm when $NaH_2PO_2{\cdot}H_2O$ is used as a reducer. With increasing MMA content in the hydrogel composition and as the nanoreactor hydrogel mesh increases, the size of the silver nanoparticles increases; the maximum absorbance decreases, and the red shifts of the peaks point to 421, 427, 433 nm, respectively, which reflects the growth of Ag particle size.

Thermal stability

In order to understand interactions between nanoparticles and the polymer matrix, thermal properties of the composite were investigated by thermogravimetric analysis (TGA). In detail, hydrogels followed two degradation steps and 89.3 wt.% degradation of the hydrogel chains occurred below 600 °C, but in the case of semi-IPN P(MMA-co-MAA)/Ag composite, it is noted as three degradation steps and only a 64.6 wt.%

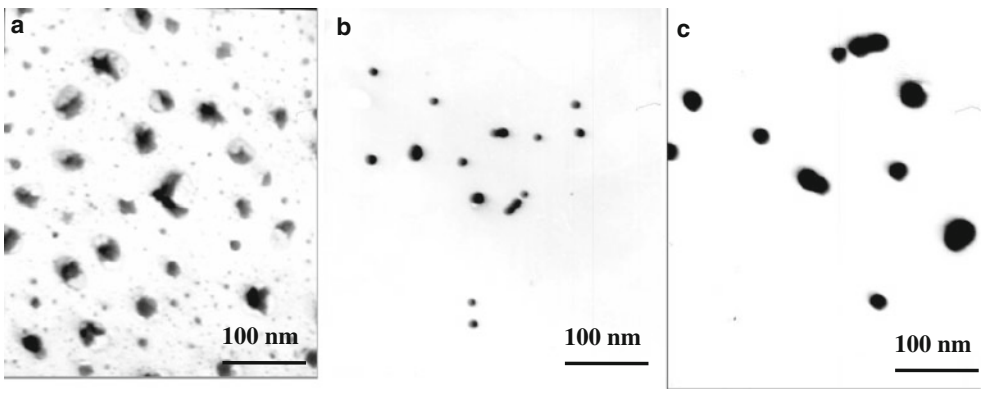

Fig. 3 TEM micrographs of Ag nanoparticles assembled in the P(MMA-co-MAA)/Ag hydrogels using $NaH_2PO_2{\cdot}H_2O$ as a reducer: **a** a direct chemical reduction avenue; **b** and **c** different mass ratios of MMA to MAA of 50:50 and 70:30, respectively

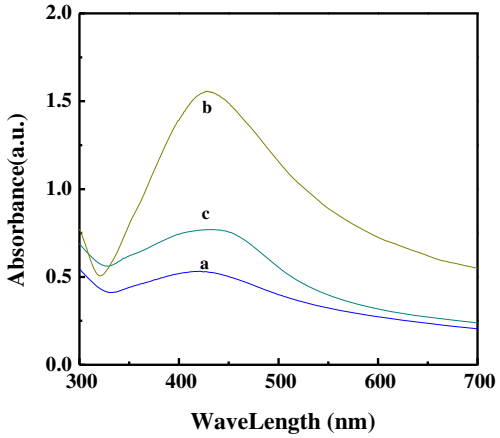

Fig. 4 UV-Vis spectra of P(MMA-co-MAA)/Ag nanocomposite hydrogels prepared from the hydrogel network, with different mass ratios of MMA to MAA: **a** 30:70; **b** 50:50; **c** 70:30

weight loss below 600 °C (Fig. 5). The weight loss difference between the semi-IPN and P(MMA-co-MAA)/Ag represents the presence of silver nanoparticles (weight percent) in the P(MMA-co-MAA)/Ag. In this particular sample, it is noted that there is a 13.7 wt.% of silver nanoparticle content in the P(MMA-co-MAA)/Ag. The onset of degradation and temperature of maximal rate of degradation in nitrogen of P(MMA-co-MAA)/Ag and pure hydrogel are higher compared with the P(MMA-co-MAA)/Ag obtained by evaporation of the solvent (H_2O) (Fig. 5). The introduction of Ag nanoparticles into the matrix has changed the degradation path of the polymer, decreasing the temperature of maximal degradation from 364 °C to 325 °C. On the other hand, the rate of degradation is lower compared with the pure hydrogel. The main decomposition products in the first step of thermal degradation of P(MMA-co-MAA) are generated by the chain-stripping elimination of H_2O, as well as cis- and trans-allylic methyls that can be formed by random chain scission reactions that accompany elimination [30]. In the second degradation step,

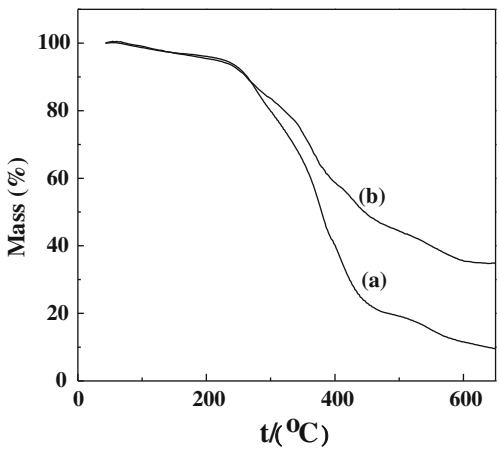

Fig. 5 The TG thermograms of **a** P(MMA-co-MAA) and **b** P(MMA-co-MAA)/Ag nanocomposite hydrogels

probably due to the network present in the polymer, the first degradation step splits into two stages, and chain-stripping elimination is followed by scission of crosslinks and chain scission reactions. When Ag nanoparticles are present in a cross-linked polymer, the interaction between nanoparticles and the polymer can occur via lone electron pairs [31, 32], inducing changes in the degradation mechanism of P(MMA-co-MAA).

Swelling studies

As shown in Fig. 6, the swelling behavior of the P(MMA-co-MAA)/Ag with various ratio of monomers in different pH buffers obviously showed pH sensitivity. In the case of high pH (7.4-11), the dominant charges in the P(MMA-co-MAA)/Ag are the dissociated carboxylate group $–CO_2^-$. In this pH region, the stronger the alkalinity of the solution, the larger the concentration of $–CO_2^-$ inside the hydrogels, which results in an osmotic pressure and makes the P(MMA-co-MAA)/Ag swell. Along with decreasing pH, the amount of $–CO_2^-$ is gradually reduced inside the hydrogels, which leads to a decrease in osmotic pressure and makes the SR of the hydrogels smaller. Therefore the SR of P(MMA-co-MAA)/Ag gradually decreased. As shown in Fig. 6, the SR was significantly increased with the rise of pH to the range of pH 3.0-11. This could be attributed to an increase of the mobile ions $–CO_2^-$ inside the hydrogel and osmotic pressure driving the gel in the swelling state. When pH<7.4, the dissociation of the carboxyl group being hindered resulted in a decrease of $–CO_2^-$ in P(MMA-co-MAA)/Ag. As shown in Fig. 6, the lowest swelling occurred almost always at pH 3.0

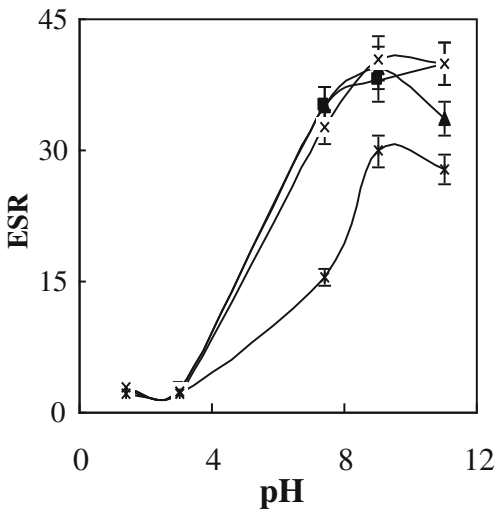

Fig. 6 Effect of different mass ratios of MMA to MAA: equilibrium water content of P(MMA-co-MAA)/Ag nanocomposite hydrogels with $NaH_2PO_2{\cdot}H_2O$ as a reducer at 25 °C. The symbols: ■, ▲, ×, and * represent the different mass ratios of MMA to MAA: 40:60, 50:50, 60:40 and 70:30, respectively

among P(MMA-co-MAA)/Ag, with various ratios of monomers. With the further lowering of pH to 1.4, the dissociation of carboxyl groups was completely inhibited. Thus, the P(MMA-co-MAA)/Ag swelled torpidly as pH diminished in the range of pH 1.4-3.0. Furthermore, the SR of the P(MMA-co-MAA)/Ag in acidic medium was obviously always smaller than that in alkaline medium [33].

Figure 7 displays time-dependent swelling behaviors of the P(MMA-co-MAA)/Ag nanocomposite hydrogels with various monomer contents in different buffer solutions. It is clear that the swelling of the hydrogels gradually increased with time, and in pH 7.4 the fastest swelling rate is observed. In this experiment, the same P(MMA-co-MAA)/Ag hydrogel samples were allowed to swell in the buffer solution, deprotonized of carboxylic acid (-COOH) groups because carboxylate anion ($COO^–$) groups can bind Ag^+ ions more tightly than -COOH groups by complexation [34, 35]. Then, the Ag^+ ions were loaded into gel network at various swelling ratios of the P(MMA-co-MAA) hydrogel to modulate the formation of Ag nanoparticles after the addition of a reducing agent $NaH_2PO_2{\cdot}H_2O$.

Furthermore, the swelling and deswelling behavior of P(MMA-co-MAA)/Ag hydrogels was investigated upon repeated immersion in pH 1.4 and 7.4 buffer solutions at 25 °C, as shown in Fig. 8. It can clearly be found that the P(MMA-co-MAA)/Ag nanocomposite hydrogels expeditiously swell in PBS solutions of pH 7.4, and simultaneously deswell rapidly in PBS solutions of pH 1.4, exhibiting good swelling and deswelling behavior. This swelling/deswelling trend is closely correlated with the protonation/deprotonation of the carboxylic acid groups in PMAA [36, 37]. At pH of 1.4, the -COOH groups are not ionized; thus, strong hydrogen bonding interactions are produced between –COOH, and the interactions between water molecules and hydrogel networks weaken or disappear. At this point, water molecules cannot diffuse into the P(MMA-co-MAA)/Ag hydrogel networks, resulting in a decreased sweling ratio. At pH

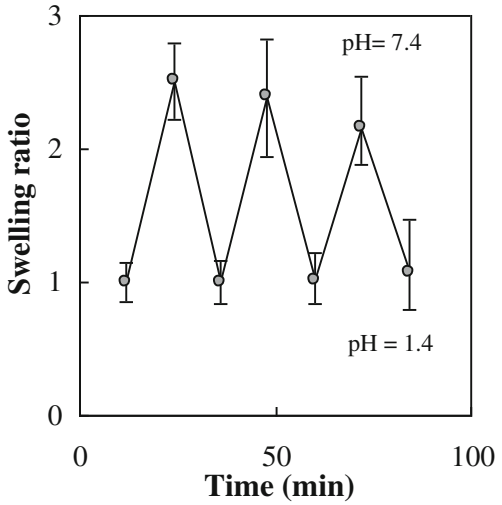

Fig. 8 Reversible swelling of P(MMA-co-MAA)/Ag hydrogels upon reopeated immersion in PBS solution of a pH 1.4 and b pH 7.4 (Ionic strength=0.2, 25 °C)

of 7.4, the -COOH groups are ionized, and the hydrogen bonding is destroyed; the charged COO^- groups repel each other, leading to swelling of the hydrogel [38, 39]. The fine swelling ratio in the P(MMA-co-MAA)/Ag composite hydrogel may be attributed to the presence of Ag colloids with surface charges in the gel network, which results in an afflux of water to balance the build-up of ion osmotic pressure. On the other hand, it is possible that some of the cross-linking gets broken during the reducing reaction, which leads to a decrease of the cross-link density. As a result, the P(MMA-co-MAA)/Ag nanocomposite hydrogels swell quickly and exhibit a goood swelling ratio.

Antibacterial studies

The bacterial effect of silver nanocomposite hydrogels mostly depends on the size of particles and the swelling ratio,

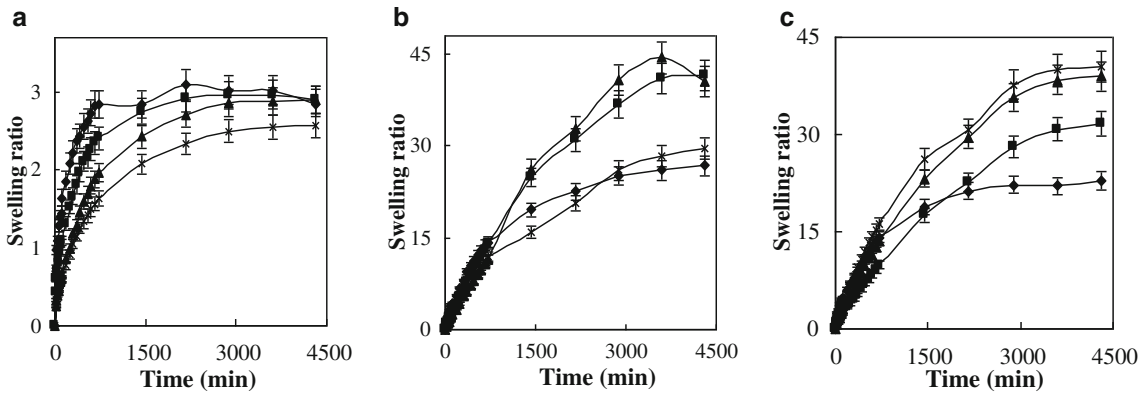

Fig. 7 Swelling ratios of various P(MMA-co-MAA)/Ag hydrogel samples in different buffer solution: **a** pH=1.4, **b** pH=7.4 and **c** pH=11.7 (The symbols: ♦, ■, ▲, and * represent the different mass ratios of MMA to MAA: 30:70, 40:60, 50:50 and 70:30, respectively)

which have a direct interaction with the bacteria [26]. As described above, an important feature of these P(MMA-co-MAA)/Ag nanocomposites is that the silver nanoparticles embedded throughout the networks are released over time in aqueous media. Therefore, the nanoparticles escape from the hydrogel networks with time and can interact with the bacteria. On the other hand, the medical effectiveness of antimicrobial agents in patients is also correleated with a certain zone size, which is used to decide whether they will be useful for treating a test pathogen. Considering a good dispersion of silver nanoparticles in hydrogels, as demonstrated by TEM observations, the antibacterial activities of a representative P(MAA-co-MMA) and P(MAA-co-MMA)/Ag sample against bacteria (*S. aureus*) were examined by the inhibitory zone test method, as shown in Scheme 1. As expected, the number of colonies grown surrounding the P(MMA-co-MAA)/Ag nanocomposites is found to be almost nil, suggesting that the P(MMA-co-MAA)/Ag nanocomposite hydrogels have excellent antibacterial activities against *S. aureus*, and the diameters of inhibitory zones for cultures are 21±1 mm. Whereas the pure P(MAA-co-MMA) hydrogel does not show any effect on *S. aureus*, and the diameter of the zone of inhibition is ca. 14±1 mm where the size of both samples is ca. 12 mm, our results suggest that pure hydrogels are generally inefficient. The antibacterial investigations against *B. subtilis* suggest the same conclusion, as the size of inhibitory zones for the nanocomposite was 19.7±1 mm, and for the pure hydrogel, it was about 13.5±1 mm. These results indicate that the P(MMA-co-MAA)/Ag nanocomposite hydrogels have a more effective contact biocidal property than the pure hydrogel.

There are two main types of hypothesis that can be used to explain the antibacterial mechanism of elemental silver. One is that the Ag nanoparticles are adsorbed at the surface of the cell membrane, causing structural damage of the cell membrane, and in turn leading to apoptosis [40]. Another is that Ag^+ ions are absorbed on the surface of the Ag nanoparticles, and the Ag^+ ions can interact with mercapto groups and amino groups, etc., of protein and DNA molecules within bacterial cells, leading the bacterial cells to lose their proliferating ability and eventually die [41]. We suggest that the antibacterial mechanism of P(MMA-co-MAA)/Ag nanocomposite hydrogels is the Ag^+ ions mechanism. Silver nanoparticles assembled in the hydrogel networks would produce silver oxide on their surface due to exposure to water and oxygen in media, which then enters into the media in the form of Ag^+ ions. Then the Ag^+ ions diffuse into the surface through the pores of the hydrogel networks and interact with the bacterial cells. It is the slow oxidation of Ag nanoparticles and slow diffusion of the Ag^+ ions through the pores of the hydrogel networks that ensure an antibacterial perdurability of the nanocomposite hydrogels. Further investigations will be made in the future; higher antimicrobial activity levels of the P(MAA-co-MMA)/Ag are expected. In a word, we conclude that the P(MMA-co-MAA)/Ag nanocomposites are excellent antibacterial materials.

Conclusion

In summary, a new P(MMA-co-MAA)/Ag nanocomposite hydrogel meant for antibacterial applications has been prepared via free radical cross-linking polymerization and follow-up reduction of silver nitrate using the hydrogel network as a nanoreactor. The nanocomposite hydrogels take on characteristic three-dimensional honeycomb topologies, as revealed by SEM observations, and slight morphological differences depend upon the copolymer composition alterations. The assembled Ag particles assume spherical-like shape in appearance at the nanoscale level, and the size of the silver nanoparticles increases with increasing MMA content in the hydrogel's composition, as disclosed by TEM and UV-Vis analyses. TGA results indicate that the P(MMA-co-MAA)/Ag nanocomposites exhibit more excellent thermostability than hydrogels. Swelling studies demonstrate that P(MMA-co-MAA) copolymer hydrogels show pH-responsive swelling behavior, and the ESR in neutral or alkaline pH solution is higher than in acidic environments. The swelling properties of the developed nanocomposites are dependent on the internal network structure and can be tuned by the feed ratios. The antibacterial activities show that the P(MMA-co-MAA)/Ag nanocomposites are excellent antibacterial materials.

Acknowledgments The authors would like to appreciate the National Science Fund for Distinguished Young Scholars of China (grant 21103146 and 21003103).

References

1. Yang Y, Shi JL, Tanaka T, Nogami M (2007) Langmuir 23:12042–12047
2. Voronov A, Kohut A, Peukert W (2007) Langmuir 23:360–363
3. Akamatsu K, Shinkai H, lkede S, Adachi S, Nawafune H, Tomita S (2005) J Am Chem Soc 127:7980–7981
4. Nguyen TH, Lee KH, Lee BT (2010) Mater Sci Eng C 30:944–950
5. Link S, El-Sayed MA (2003) Annu Rev Phys Chem 54:331–335
6. Maneerung T, Tokura S, Rujiravanit R (2008) Carbohydr Polym 72:43–51
7. Anshupriya S, Sounak D, Subhabrata M, Prasanta KD (2011) Soft Matter 7:3011–3022
8. Mohan YM, Lee K, Premkumar T, Geckeler KE (2007) Polymer 48:158–164
9. Babu R, Zhang J, Beckman EJ, Virji M, Pasculle WA, Wells A (2006) Biomaterials 27:4304–4314
10. Xia HY, Zhang Y, Sun S, Fang Y (2007) Colloid Polym Sci 285:1655–1663
11. Zeng R, Rong MZ (2001) J Mater Sci Lett 20:1473–1476

12. Chung YC, Chen IH, Chen CJ (2008) Biomaterials 29:1807–1816
13. Jin WJ, Jeon HJ, Kim JH, Youk JH (2007) Synth Met 157:454–459
14. Shin J, Kim Y, Lee K, Lim YM, Nho YC (2008) Phys Chem 77:871
15. Wang C, Flynn NT, Langer R (2004) Mater Res Soc Symp Proc 820: R2.2.1
16. Hon Ho C, Tobis J, Sprich C, Thomann R, Tiller JC (2004) Adv Mater 16:957–961
17. Furno F, Morley KS, Wong B, Sharp BL, Arnold PL, Howdle SM, Bayston R, Brown PD, Winship PD, Reid HJ (2004) J Antimicrob Chem 54:1019–1024
18. Sobczak-Kupiec A, Malina D, Piatkowski M, Krupa-Zuczek K, Wzorek Z, Tyliszczak B (2012) J Nanosci Nanotechnol 12:9302–9311
19. Agnihotri S, Mukherji S, Mukherji S (2012) Appl Nanosci 2:179–188
20. Hebeish A, Hashem M, Abd El-Hady MM, Sharaf S (2013) Carbohydr Polym 92:407–413
21. Peppas NA, Khare AR (1993) Adv Drug Deliv Rev 11:1–35
22. Dhandayuthapani B, Yoshida Y, Maekawa T, Kumar DS (2011) Int J Polym Sci 2011:89–108
23. Donini C, Robinson DN, Colombo P, Giordano F, Peppas NA (2002) Int J Pharm 245:83–91
24. Gan Z, Ju J, Zhang T, Wu D (2011) J Nanomater 2011:231–238
25. Foss CA, Peppas NA (2004) Eur J Pharm Biopharm 57:447–455
26. Chandra Babu A, Prabhakar MN, Suresh Babu A, Mallikarjuna B, Subha MCS, Chowdoji, Rao K (2013) J Carbohydr Chem 2013:1–8
27. Xiang YQ, Chen DJ (2007) Eur Polym J 43:4178–4187
28. Yao SW, Liu HQ, Zhang HZ, Zheng CF (2003) Acta Phys -Chim Sin 19:464
29. He J, Kunitake T, Nakao A (2003) Chem Mater 15:4401–4406
30. Henglein A (1993) J Phys Chem B 97:5457–5471
31. Gilman JW, Van der Hart DL, Kashiwagi T (1994) ACS Symp Ser 599:21
32. Krklješ A, Nedeljković JM, Kačarević-Popović ZM (2007) Polym Bull 58:271–279
33. Lin YW, Chen Q, Luo HB (2007) Carbohydr Res 342:87–95
34. Ung T, Liz-Marzàn LM, Mulvaney P (1999) J Phys Chem B 103: 6770–6773
35. Van Hyning DL, Zukoski CF (1998) Langmuir 14:7034–7046
36. Fernyhough C, Ryan AJ, Battaglia G (2009) Soft Matter 5:1674–1682
37. Laleh S, Mohammad A, Azizollah N, Mohammad I (2012) Dent Mater 28:1041–1050
38. Shalviri A, Chan HK, Raval G, Abdekhodaie MJ, Liu Q, Heerklotz H (2012) Colloids Surf B 101:405–413
39. Zhang C, Han HM, Qu P, Xu J, Zhou Y, Wang J (2013) Adv Mater Res 627:730–733
40. Sondi V, Salopek-Sondi B (2004) J Colloid Interface Sci 275:177–182
41. Lok CN, Ho CM, Chen R (2007) Chem 12:527–534